# Optimization in interstitial plasmonic photothermal therapy for treatment planning

Ravi Kumar Kannadorai and Quan Liu[a)]
*Division of Bioengineering, School of Chemical and Biomedical Engineering, Nanyang Technological University, Singapore 637457*

(Received 12 September 2012; revised 29 April 2013; accepted for publication 16 May 2013; published 5 September 2013)

**Purpose:** Gold nanorods have the potential to enhance the treatment efficacy of interstitial photothermal therapy. In order to enhance both the potential efficiency and the safety of such procedures, treatment planning on laser power density, nanoparticle concentration, and exposure time has turned out to be useful in predicting the thermal damage and optimizing treatment outcome. To the best of our knowledge, there is no previous report on the optimization of interstitial plasmonic photothermal therapy (PPTT) for all these free parameters simultaneously. The authors propose to develop a suitable optimization algorithm for interstitial PPTT to optimize these parameters and achieve complete damage to spherical tumors of different sizes with a damage margin width of 1 mm from the tumor boundary embedded deep inside a normal tissue model.

**Methods:** In a numerical tissue model, the standard Pennes bioheat equation and the first-order thermal–chemical rate equation were used to model the temperature and thermal damage distributions, respectively, in spherical tumors that were embedded deep inside a normal tissue and incubated with nanorods. The concentration of nanorods in the normal tissue was set to be about one quarter of that in the tumor. Thermal damage due to varying concentrations of nanorods, laser power density, and exposure time was computed for a series of tumor radii including 2, 3, 4, and 5 mm. An optimization algorithm was developed to determine the optimum laser power density, nanorod concentration, and exposure time for the treatment of such spherical tumors. In this algorithm, a novel objective function was created to enable the optimization of multiple key parameters, including nanoparticle concentration, power density, and exposure time, simultaneously to achieve not only the complete thermal damage to the entire tumor but also the collateral damage to the surrounding normal tissue with a margin width of 1 mm from the tumor boundary. Different weights were assigned sequentially to each free parameter according to the relative importance of the parameters. A thermal damage value of one calculated by Arrhenius damage law, which is more accurate than a threshold temperature typically used for characterizing thermal damage, was used to indicate effective treatment.

**Results:** The simulation results show that there is a steady increase in the overall temperature as the nanorod concentration increases; however, the uniformity of the temperature distribution changes significantly which in turn affects the thermal damage. Optimization results show that any slight decrease in one free parameter can be compensated by the increase in other free parameters, in which the complete thermal damage of the tumor and the collateral damage to normal tissue with a margin width of 1 mm can be always achieved. This implies the importance of optimization in interstitial PPTT.

**Conclusions:** The proposed method can optimize laser power density, nanoparticle concentration, and exposure time simultaneously with different weights in interstitial PPTT planning for deep seated tumors. It provides flexibility for a clinician to make appropriate planning for individual patients according to their special needs.  [http://dx.doi.org/10.1118/1.4810935]

Key words: bioheat transfer, thermal damage, finite element method, nanorods, optimization, photothermal therapy

## 1. INTRODUCTION

Plasmonic photothermal therapy (PPTT) has attracted significant attention because of the merits of nanoparticles in photostablility, photobleaching, and enhanced absorption cross sections.[1] Compared to conventional laser therapy, it could be used to selectively heat the local medium by converting the photon energy into heat and diffusing it out to its surrounding medium. Nanoparticle mediated photothermal therapies are predominantly designed to operate in "NIR window" to minimize attenuation of the energy resulting from undesired light–tissue interactions, and to prevent undesirable damage due to heating of healthy tissue. NIR absorbing nanoparticles[2] have been successfully demonstrated for the treatment of human

breast epithelial cancer,[3] prostate cancer,[4] oral squamous cell carcinoma,[5] and colon cancer[6] xenografted into mice. Though nanoparticles seem to have a good potential, multiple treatment conditions must be carefully manipulated in order to achieve an effective PPTT treatment. Manipulation of treatment conditions, which interact with each other nonlinearly, includes selecting the proper laser wavelength, power, and exposure time (ET), selecting the proper type and placement of fibers/applicators, and selecting the type and concentration of nanoparticles.

For those tumors located deep underneath the tissue surface, interstitial PPTT is more advantageous than PPTT with superficial illumination. Interstitial PPTT is an extension of laser-induced interstitial thermotherapy (LITT), which is a minimally invasive local laser thermal treatment. LITT has been used clinically to treat tumors and other diseases in organs such as the liver,[7] brain,[8] prostate,[9] and breast.[10] In LITT, near-infrared laser radiation is delivered to the targeted tissue volume via an optical fiber delivery system to achieve tissue necrosis to ensure total cancer cell death and minimize damage to surrounding healthy tissue, especially in vital organs during the treatment. Although the development of interstitial PPTT is still in its early stage, it can be anticipated that interstitial PPTT may become as popular as LITT in the near future.[11]

Numerical modeling of the laser–tissue interaction process is an important and effective way to facilitate the evaluation of a wide range of parameters for a desired outcome without extensive *in vivo* trials. A number of early studies have sought to model the hyperthermic and coagulative responses of tissues during surface-irradiation[12,13] and laser interstitial thermal therapy processes[14,15] without the use of nanoparticles. Conventional modeling has normally included the following three steps: (1) calculation of the laser energy distribution using various optical models; (2) calculation of the temperature increase using bioheat transfer equation; and (3) calculation of the extent of the thermal damage. The same techniques have been extended to simulate nanoparticle-mediated laser surgical protocols. Elliott *et al.*[16] modeled and demonstrated experimentally on phantoms the spatiotemporal thermal distribution associated with surface-irradiation of near-infrared laser combined with gold nanoshells, which was later demonstrated on animals.[17] Their methods mainly focus on the use of two different concentrations of nanoparticles to demonstrate the extent of spatial distribution in light absorption and calculate the subsequent temperature field for a set of laser powers in external illumination. For deep seated tumors, Xiao *et al.*[18] numerically investigated the effect of varying concentrations of nanoshells on the optical and thermal distribution in interstitial laser therapy for relatively large tumors. Though these works yield useful tools to predict the temperature profiles for a set of laser power and nanoparticle concentrations (NC), they did not explore the optimization of laser thermal therapy through systematic evaluation of contributing parameters.

Optimization algorithms for laser treatment planning have been investigated previously by several other groups. In photothermal therapy Rylander *et al.*[19,20] developed an optimization algorithm for prostate cancer laser therapy design which focuses on achieving maximum prostate tumor destruction and minimizing injury to healthy surrounding tissue. In this work, the optimization process is driven through the minimization of objective functions based on desired heat shock protein (HSP) expression and injury fraction. This work was further extended to build a computational model of the bioheat transfer in living tissue to guide, in real-time, laser treatment of prostate cancer monitored by magnetic resonance thermal imaging where three different objective functions were developed to optimize the temperature, damage, and HSP, respectively.[21] These optimization techniques use a different objective function to optimize each quantity, which makes the use of such optimization complicated. Extending the optimization process to nanoparticle mediated laser surgery, Feng *et al.*[22] presented an integrated computer model using an optimization algorithm to simulate laser surgery and provide transient temperature field predictions. They developed a nested-block optimization algorithm that is applied to the Pennes bioheat transfer model[23] to simulate the transient temperature field during laser surgery on a prostate tumor by taking the difference between the computed temperature field and the measured temperature field. Though this method predicts the optimum temperature and its distribution in the tumor region, it fails to systematically evaluate the importance of each free parameter on thermal damage. Because PPTT involves several key parameters such as laser power density (LPD), nanoparticle concentration (NC), and exposure time (ET) which can all affect the treatment outcome, it is important to develop an optimization strategy to take all these parameters into account in order to achieve the optimal outcome with minimal adverse effect on patients. There is no previous report on optimizing all these free parameters for damaging the tumor of interest and at the same time minimizing the damage to the normal tissue in PPTT to the best of our knowledge.

We propose to develop a suitable optimization algorithm for interstitial PPTT to completely damage spherical tumors of different sizes plus an additional 1 mm of the normal tissue surrounding the tumor to prevent the regrowth of tumor. We will use Pennes bioheat equation[23] and Arrhenius damage law[24] to determine the temperature and thermal damage distributions, respectively. Then through a systematic optimization strategy with a novel tunable objective function, we obtain the optimized parameters for achieving complete thermal damage for different tumor sizes. As compared to other previous reports, our approach is novel in (1) taking into consideration all three key parameters in a single objective function including laser power density, nanoparticle concentration, and exposure time with weights accounting for the relative importance of each parameter and (2) using complete thermal damage calculated from Arrhenius damage law[24] that corresponds to irreversible thermal damage to tissues instead of a threshold temperature value as the end point to indicate thermal damage. This optimization based treatment planning platform would allow clinicians to select parameter values and predict the thermal damage in interstitial PPTT. It can be a useful tool to show the thermal damage profiles for tumors with various

sizes. The implementation of this information has a potential to reduce the complexity of treatment planning and provides means to deliver more conformal thermal damage.

## 2. COMPUTATIONAL METHODS

The computational model takes into account interstitial laser illumination, thermal propagation, and thermal damage due to embedded gold nanorods in a tumor buried in a homogenous normal tissue. The model consists of two steps of computation. First, temperature elevation will be calculated as a result of heat generation due to gold nanorods embedded in tissue via photothermal effect. Second, the thermal damage is calculated from the history of temperature rise at each location. Since the optical properties of the tumor region can be altered by adjusting the concentration of nanorods, the tumor absorption coefficient can be controlled to achieve effective and selective heating of the tumor. Each step of the modeling process is described in Secs. 2.A and 2.B.

### 2.A. Bioheat distribution

The Pennes bioheat equation[23] describes the heat diffusion in a tissue caused by heating from any source. Heat was generated from the absorption of light energy in this particular study. The governing equation in a cylindrical coordinate system is as shown below:

$$\rho C_p \frac{\partial T}{\partial t} = k\left[\frac{1}{r}\frac{\partial}{\partial r}\left(r\frac{\partial T}{\partial r}\right) + \frac{\partial^2 T}{\partial^2 Z}\right] + \rho_b C_{p,b}\omega_b(T_b - T) + Q_m + Q, \quad (1)$$

where $\rho$ $C_p$ and $k$ correspond to the density (kg m$^{-3}$), specific heat (J kg$^{-1}$ K$^{-1}$), and thermal conductivity (W m$^{-1}$ K$^{-1}$) of the medium, respectively. $\rho_b$, $C_{p,b}$, and $\omega_b$ correspond to the density, specific heat, and perfusion rate of blood, respectively. $T_b$ and $T$ correspond to the arterial blood temperature (°C) and temperature (°C), respectively. $Q_m$ is the metabolic heat source term. In addition, $Q$ is the external heat source term, which for a cylindrical laser applicator is defined as[25,26]

$$Q = \frac{k_\alpha I_O e^{-k\alpha r}}{r^{1/2}}, \quad (2)$$

where $k_\alpha$ is the absorption coefficient (m$^{-1}$), $I_O$ is the laser power density (W m$^{-3}$), and $r$ is the radial distance from the center of the applicator (m).

At the boundaries, the tissue is assumed to be at the arterial blood temperature ($T_b$) which is normally assumed to be fixed at 37 °C. The initial temperature inside the tissue and the tumor is also kept at 37 °C mimicking the normal body temperature.

As the laser light propagates through nanoparticle incubated biological tissues, it is absorbed by the nanoparticle and also by the tissue. Therefore, $k_\alpha$ should be the overall contribution due to absorption from both the biological tissue ($k_t$) and the embedded nanorods ($k_{nr}$):

$$k_\alpha = k_{nr} + k_t. \quad (3)$$

For nanorods, $k_{nr}$ can be quantified[27,41] in terms of the absorption efficiency (ratio of its absorption cross section to the total cross-sectional area of the nanorod),[28] $Q_{abs}$, and the number of nanorods per unit volume, $N_T$:

$$k_{nr} = \pi r_{\text{eff}}^2 Q_{\text{abs}} N T, \quad (4)$$

where $r_{\text{eff}}$ is the effective radius of the nanorod which can be calculated from its Volume $V$ and is given by

$$r_{\text{eff}} = \left(\frac{3V}{4\pi}\right)^{1/3}. \quad (5)$$

### 2.B. Thermal damage

Thermal damage in cells and tumor can be predicted mathematically by a first-order thermal–chemical rate equation, in which temperature history determines the damage. Damage is considered to be a unimolecular process, where native molecules transform through an activated state leading to cell death. Damage is quantified using a single parameter Ω and is calculated from Arrhenius law.[24] Damage Ω is dimensionless, exponentially dependent on temperature, and linearly dependent on time of exposure, which is given by

$$\Omega(\tau) = \ln\left(\frac{C_0}{C_\tau}\right) = A_f \int_0^\tau \exp\left(\frac{-E_a}{RT(t)}\right) dt, \quad (6)$$

where Ω is defined as the logarithmic of the ratio of initial concentration of healthy cells, $C_0$, to the fraction of healthy cells, $C_\tau$, at time $\tau$. $A_f$ (s$^{-1}$) is the frequency factor, $E_a$ (J mole$^{-1}$) is the injury process activation energy, $R$ (J mole$^{-1}$ K$^{-1}$) is the universal gas constant, and $T$ (K) is the instantaneous absolute temperature of the cells during thermal stress which is a function of time, $t$ (s). Equation (6) indicates that the measure of damage (Ω) describes the probability of tissue being destroyed. It is the logarithm of the ratio of the initial concentration of undamaged tissue to the concentration once damage has accumulated, for the time interval $t = 0$ to $t = \tau$. As used previously in the literature,[29,30] $\Omega = 1$ is chosen in this study to indicate that a sufficient irreversible damage has been achieved.

The simulation model for interstitial PPTT of RCC is as shown in Fig. 1. The laser/tumor/tissue system was modeled and relevant equations were solved numerically using the finite element modeling (FEM) method by a commercial FEM package (COMSOL Multiphysics 4.2). Using this software, the bioheat transfer equation and the thermal damage function were calculated simultaneously. Since the model is axisymmetric, a 2D axisymmetrical[31] model was setup to simplify and speed up the simulation. The model basically consists of a cylindrical tissue 50 mm in length and a radius of 25 mm in which a spherical tumor of radius $R$ is embedded. The simulations were performed on tumors of a series of radii including 2, 3, 4, and 5 mm.

The transient heat conduction equation[30] in COMSOL was solved to obtain the temperature inside the domain using the geometry as shown in Fig. 1. In the model a cylindrical laser diffuser of 1 mm in diameter, with a radial illumination length of $2R$ and an additional 1 mm in the either side of the axial dimension in the tumor as shown in Fig. 1 to achieve a

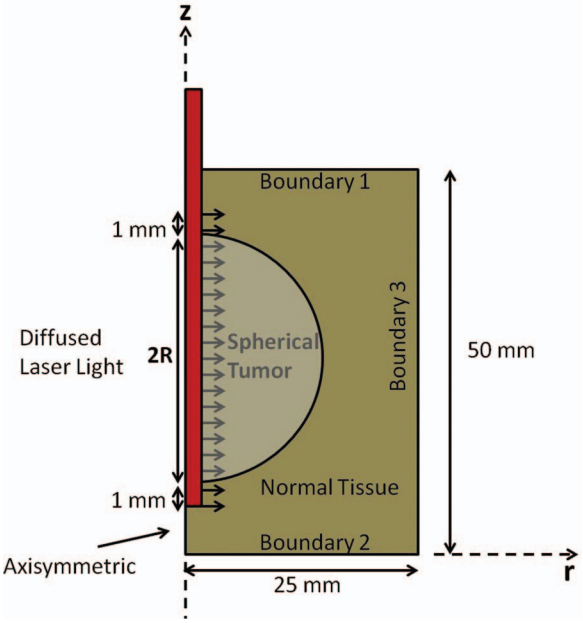


FIG. 1. Schematic of interstitial plasmonic photothermal therapy showing the cross section of a spherical tumor embedded in normal tissue used for simulating the spatiotemporal temperature distribution and thermal damage. Only half of the cross section is shown due to the axisymmetry around the z-axis. The short arrows in the tumor area indicate the direction of light illumination from the diffuser (1 mm in diameter and R + 2 mm in length). The diffuser is shown for illustration purpose only. Boundaries 1, 2, and 3 are maintained at the arterial blood temperature ($T_b$) which is fixed at 37 °C in this study.

more uniform thermal damage was assumed to be already inserted into the tumor. Throughout the simulation a 785 nm near-infrared laser light with a power density varying from 0 W m$^{-3}$ to 3 × 10$^3$ W m$^{-3}$ emanating from the surface of the cylindrical laser diffuser was considered. The laser exposure time was varied from 0 to 900 s to observe tissue damage at different time points. The upper limits of the laser power density and exposure time were selected to include the typical values used in photothermal therapy.[5] Gold nanorods with 10 nm axial diameter and 38 nm in length were used in the interstitial PPTT model. These nanorods have longitudinal surface plasmon resonance (SPR) at 780 nm, an absorption cross section of 3 × 10$^{-15}$ m$^{-2}$, and an absorption efficiency of 45.[28] The plasmon resonance wavelength of these nanorods closely match with the laser wavelength.

The nanorods were assumed to be injected intravenously before PPTT. When injected intravenously these nanorods get accumulated and retained in the tumor interstitial space mainly through the enhanced permeability and retention (EPR) effect and also in the surrounding normal tissue[32] and in other organs such as liver, spleen, and lungs. The gold concentration in the tumor is three or four times that of the surrounding normal tissue.[32,33] For example, if we assume that the nanorod concentration in the tumor is 1 × 10$^9$ nps/ml, in which "nps" is the abbreviation of "nanoparticles," then the nanorod concentration in the surrounding normal tissue would be ~0.29 × 10$^9$ nps/ml. And hence, according to Eq. (3) the nanorods will contribute to an increase in $k_\alpha$ in the tumor and the tissue region. The nanorod concentration was varied from 0 to 7.5 × 10$^9$ nps/ml in the simulations; any further increase in the concentration had little effect on the thermal damage.

TABLE I. List of input parameters used in the simulation of bioheat transfer and thermal damage function in COMSOL Multiphysics.

| Parameter | Value |
|---|---|
| Tissue/tumor: thermal conductivity, $k$ (Ref. 36) | 0.5 W m$^{-1}$ K$^{-1}$ |
| Tissue/tumor: density, $\rho$ (Ref. 36) | 1050 kg m$^{-3}$ |
| Tissue/tumor: specific heat, $C_p$ (Ref. 37) | 3900 J kg$^{-1}$ K$^{-1}$ |
| Blood: density, $\rho$ (Ref. 38) | 1100 kg m$^{-3}$ |
| Blood: specific heat, $C_p$ (Ref. 38) | 3600 J kg$^{-1}$ K$^{-1}$ |
| Metabolic heat generation, $Q_m$ | |
| Tissue (Ref. 39) | 700 W m$^{-3}$ |
| Tumor (Ref. 39) | 65 400 W m$^{-3}$ |
| Blood perfusion rate, $\omega_b$ | |
| Normal renal cortex (Ref. 34) | 454.32 ml/min/100 g |
| Renal cell carcinoma (Ref. 34) | 261.96 ml/min/100 g |
| Arterial blood temperature, $T_b$ | 37 °C |
| Initial tissue temperature, $T_i$ | 37 °C |
| Frequency factor ($A_f$) (Ref. 40) | 2.84 × 10$^{99}$ s$^{-1}$ |
| Activation energy ($E_a$) (Ref. 40) | 6.18 × 10$^5$ J/mole |
| Universal gas constant | 8.3 J/mole/K |

For simulating thermal damage, the transient diffusion equation[30] in COMSOL was used. The diffusion coefficient of the equation is set to zero and the source term of the diffusion is set as $A_f \exp[-E_a/RT(t)]$. The boundary condition of the diffusion equation is set as insulation (flux = 0) at all the boundaries. The thermal damage contour levels were plotted in the domain at the end time. The region within the innermost contour ($\Omega = 1$) is said to have been thermally damaged.

This treatment procedure was mainly focused for the treatment of renal cell carcinoma (RCC) and hence the optical and thermal properties corresponding to the kidney were used in the simulation.[34] Since biological tissues are mostly transparent in the therapeutic optical window, the absorption coefficients ($k_t$) of the tumor (RCC) and the surrounding normal tissue (kidney) in this spectral region were quite low, which were chosen to be 8 and 25 m$^{-1}$, respectively, according to the literature.[35] In all the calculations, it was assumed that only the optical properties of the tissue model including the tumor were affected by the gold nanorods. The physical and thermal properties such as the density and specific heat were assumed not varying with the addition of nanorods. The values of parameters used in the simulation of bioheat transfer and thermal damage are summarized in Table I.

## 2.C. Optimization scheme

In any hyperthermia treatment for tumor, one would always desire the complete necrosis of the tumor region plus an additional 1 mm of the normal tissue from the tumor boundary while minimizing damage to the rest of the normal tissue. Such a goal is achieved by ensuring that the radius corresponding to complete thermal damage obtained from Arrhenius law covers the entire tumor and small section of the normal tissue.

A constrained optimization problem was developed with the following free parameters, i.e., LPD, ET, and NC. The problem was formulated as follows:

$$\min f(\text{LPD, ET, NC}) = \sum_{i=1}^{3} W_i \left( \frac{x_i - \text{lb}_i}{\text{ub}_i - \text{lb}_i} \right)^2 \quad (7)$$

with an equality constraint of

$$\text{TDR} - (R + 1\,\text{mm}) = 0,$$

where TDR corresponds to the simulated minimum radius corresponding to complete thermal damage, $R$ represents the actual tumor radius for which an additional 1 mm is taken for the collateral damage, $x = [\text{LPD, ET, NC}]$, $W$ is the weight factor, and lb and ub correspond to the lower bound and upper bound values of each variable, respectively. It can be seen that the optimization result from Eq. (7) would yield minimal values in the laser power density, exposure time, and nanoparticle concentration, while the constraint would ensure a reasonable treatment outcome, which is desirable in a typical PPTT procedure. In Eq. (7), each free parameter in the minimization problem can be weighted differently according to a user's preference.

During optimization, the lower bound (lb) and upper bound (ub) values were 0 and $3.0 \times 10^3$ W m$^{-3}$, 0 and 900 s, 0 and $7.5 \times 10^9$ nps/ml for LPD, ET, and NC, respectively. The parameter values that induced a collateral damage to the normal tissue with a margin of at least 2 mm ($\Omega = 1$) from the tumor boundary were taken as the upper bounds. The optimization process was carried out for different sets of weights for individual parameters to evaluate how the optimization result varies with the weight set. In this study, a weight value of 100 to 20 in steps of 20 was assigned to a free parameter depending on whether the minimization of the parameter was considered important or less important. Hence, a total of 125 different weight sets for each tumor size were evaluated. The optimization problem was then solved using a function, *fmincon*, in the Optimization Toolbox of MATLAB 11 (Mathworks, Inc., Natick, MA, US), which attempts to find a constrained minimum of a scalar function of several variables starting at an initial estimate. For those values of free parameters not simulated, the *interp3()* function in MATLAB was used to interpolate and perform optimization.

## 3. RESULTS

Numerous simulations were conducted to investigate the effects of inclusion of nanorods on the temperature and the damage function. To investigate the effect of laser power density with zero concentration of nanorods, the tissue/tumor model was simulated and results are as shown in Fig. 2. The laser power density was steadily increased and at the same time the model was exposed to a sufficiently large time. The results show that there is hardly any increase in overall temperature of the tumor. Figure 3 compares the temperature distribution in a tumor having a uniform distribution of nanorods with various concentrations induced by a laser at a power density of $3 \times 10^3$ W m$^{-3}$. There is a steady increase in the overall temperature as the concentration increases; however,

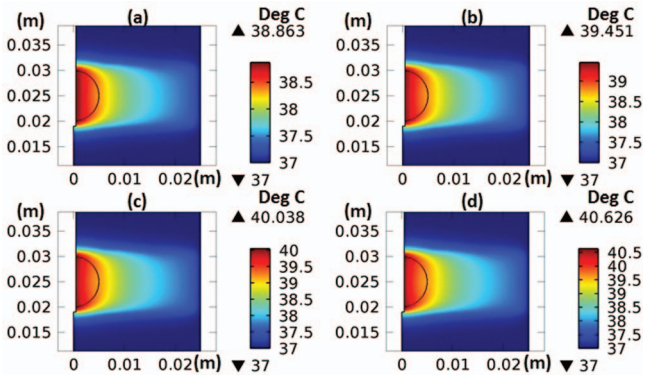


FIG. 2. Temperature distribution with no nanorods in a 5-mm radius tumor model exposed (900 s) to a laser power density of (a) $1.5 \times 10^3$, (b) $2 \times 10^3$, (c) $2.5 \times 10^3$, and (d) $3 \times 10^3$ W m$^{-3}$. The units of both x and y axes are meters and the unit of temperature is °C.

the uniformity of the temperature distribution changes significantly. It can be observed that the temperature distribution is squeezed toward the laser diffuser as the concentration of nanoparticles increases, which suggests that thermal damage occurs in a shallower tissue region.

Figure 4 gives a detailed graph about how the concentration of nanorods affects the temperature along the radius of the tumor and the tissue. It is clear that the temperature next to the diffuser increases with an increasing nanoparticle concentration. Irrespective of the concentration, the temperature drastically decreases from the diffuser (zero radius) to the boundary of tumor and tissue and eventually equals the initial temperature (37 °C). It is also noted that the slope of the decreasing trend increases with the nanoparticle concentration, which could be attributed to the increasing absorption due to nanoparticles.

Figure 5 shows the thermal damage contours that are overlaid on the temperature distribution profiles at an exposure time of 900 s, in which the laser density and nanorod concentration are $2.5 \times 10^3$ W m$^{-3}$ and $4 \times 10^9$ nps/ml, respectively, for a series of tumor radii including 2, 3, 4, and 5 mm. For a

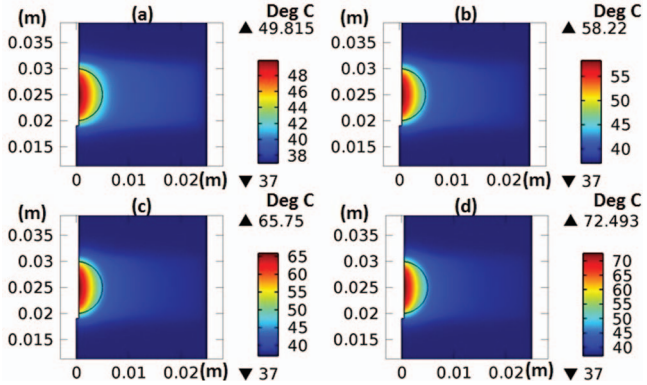


FIG. 3. Temperature distribution in the tumor model for a range of nanorod concentrations for a tumor with a 5-mm radius (R) illuminated by a diffuser of length 2R +2 mm. The units of both x and y axes are meters and the unit of temperature is °C. The laser power density is $3.0 \times 10^3$ W m$^{-3}$ and the exposure time is 900 s. The concentrations covered include (a) $2.5 \times 10^9$, (b) $5.0 \times 10^9$, (c) $7.5 \times 10^9$, and (d) $10.0 \times 10^9$ nps/ml.

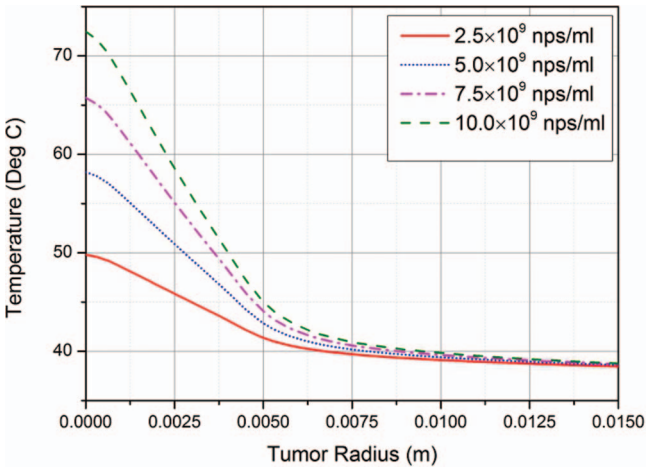


FIG. 4. Temperature distribution along the radius (5 mm) in the tumor model for various concentrations of nanorods ($2.5 \times 10^9$–$10.0 \times 10^9$ nps/ml) exposed to a laser power density of $3.0 \times 10^3$ W m$^{-3}$ for 900 s.

successful thermal therapy the entire tumor should be within the thermal damage contour. The tumor boundary represented by the thick black line is within the innermost contour ($\Omega = 1$) for all the tumor sizes which signifies that the tumor of interest has been completely damaged. When the thermal damage contour is close to the tumor boundary, it mimics the shape of the tumor boundary, i.e., a circle. So the radius of the contour corresponding to complete thermal damage ($\Omega = 1$) can be used to approximately represent the spatial extent of effective treatment.

The optimization result for a weight value of 100 or 50 assigned to the free parameter is listed in Table II. By comparing a pair of results for different weight sets, for example, the first and second sets in which the weight of LPD is larger in the first set than in the second set while other weights are equal in two sets, it can be seen that the assignment of a larger

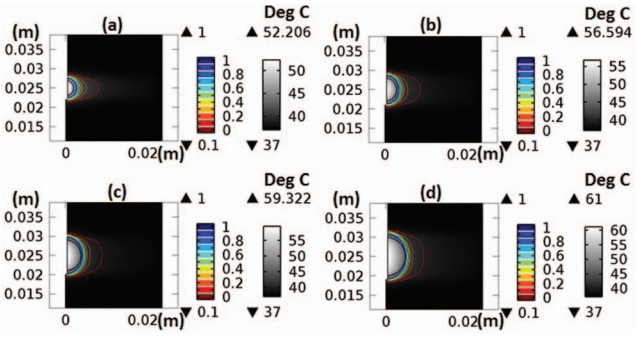


FIG. 5. Thermal damage profiles obtained by solving the first-order rate equation for a laser power density of $2.5 \times 10^3$ W m$^{-3}$, nanoparticle concentration of $4 \times 10^9$ nps/ml, and exposure time of 900 s. The regions within the inner most contour encircling the tumor boundaries (thick black line) correspond to $\Omega = 1$, which are considered to have undergone irreversible cell damage. Panels (a)–(d) show the thermal damage to tumors of radii R equal to 2, 3, 4, and 5 mm, respectively, using a diffuser of length 2R + 2 mm with 1 mm on either side of the axial dimension in the tumor. The units of x and y axes are meters and the unit of temperature is °C. The first color bar corresponds to the thermal damage contours and the second grey scale bar corresponds to temperature in each figure.

weight to a free parameter does result in a smaller value in the optimization result as expected. As a tradeoff, the other two free parameters have to take larger values for compensation to achieve similar treatment outcome. This demonstrates the effectiveness of the weighting scheme.

The data from Table II and the optimization data corresponding to the weight values of 100 to 20 in steps of 20 are plotted in a color mapped 2D scatter plot for better comparison and visualization as shown in Fig. 6, in which the color map in the plot represents the laser power density. The data corresponding to Table II are highlighted and the results are mostly concentrated in the middle suggesting that different weights, i.e., 100 or 50, could result in a significant change in the results of optimization. By comparing a pair of results for different weight sets, for example, the first and second sets in which the weight of LPD is 100 in the first set and 50 in the second set, it can be seen that the assignment of a small weight to a free parameter does result in a higher value for LPD which in turn results in a smaller value for ET and NC in the optimization result. This demonstrates the effectiveness of the weighting scheme. Furthermore, it can be seen in Fig. 6 that the optimized result could change significantly with the weight combination, which indicates that a clinician could have a quite large freedom to select these parameters for individual patients while still achieving the desired treatment outcome.

## 4. DISCUSSION

Figure 2 shows that varying laser power density and exposing it for a sufficiently long time have a moderate effect on the overall temperature rise with zero concentration of nanorods because of the low absorption coefficient in the tumor/tissue model. Adding nanorods increases the absorption coefficient which will dramatically alter the overall heat generation and distribution in the model, which can be seen from the significant increase in the maximum temperature in Fig. 3. It is interesting to note that an increase in nanorod concentration creates a less penetrating temperature profile as shown in Fig. 3. Because the nanorods in this study possess strong absorption and weak scattering, the decrease in the penetration depth of thermal damage could be mainly attributed to the increased light absorption as the concentration increases. This finding agrees with the previous reports, where it is shown how the laser penetration depth[41] was decreased and the temperature distribution[42] was shrunk in the presence of nanoparticles. This observation implies the importance of finding optimal nanoparticle concentration to achieve thermal damage down to a desired depth. In Fig. 4, it can be observed that the temperatures at the tumor boundary and beyond are similar irrespective of the concentration of nanorods. This is mainly due to the removal of heat by blood perfusion, which plays a significant role in heat and mass transfer of a biological medium.[43,44]

For a successful therapy and to prevent any reoccurrence of a malignant tumor, a marginal collateral damage to the normal tissue is desired by clinicians. Figure 5 suggests that the required collateral damage to remove the positive margins

TABLE II. Optimized values of free parameters for a series of weight sets to achieve complete thermal damage to tumors of different sizes. A weight of 100 corresponds to "highly important" and 50 corresponds to "can be compromised."

| Weights | | | | Tumor | | | |
|---|---|---|---|---|---|---|---|
| LPD | ET | NC | Parameter | R = 2 mm | R = 3 mm | R = 4 mm | R = 5 mm |
| 100 | 100 | 100 | LPD ($\times 10^3$ W m$^{-3}$) | 2.83 | 2.58 | 2.63 | 2.62 |
| | | | ET (s) | 449 | 649 | 698 | 707 |
| | | | NC ($\times 10^9$ nps/ml) | 4.70 | 5.50 | 5.50 | 5.40 |
| 50 | 100 | 100 | LPD ($\times 10^3$ W m$^{-3}$) | 3.00 | 3.00 | 3.00 | 3.00 |
| | | | ET (s) | 392 | 564 | 614 | 618 |
| | | | NC ($\times 10^9$ nps/ml) | 4.20 | 4.70 | 4.90 | 4.80 |
| 100 | 50 | 100 | LPD ($\times 10^3$ W m$^{-3}$) | 2.67 | 2.39 | 2.41 | 2.39 |
| | | | ET (s) | 610 | 811 | 861 | 870 |
| | | | NC ($\times 10^9$ nps/ml) | 4.80 | 5.10 | 5.10 | 5.00 |
| 100 | 100 | 50 | LPD ($\times 10^3$ W m$^{-3}$) | 2.25 | 2.28 | 2.48 | 2.48 |
| | | | ET (s) | 409 | 585 | 667 | 679 |
| | | | NC ($\times 10^9$ nps/ml) | 7.50 | 7.50 | 6.60 | 6.40 |
| 100 | 50 | 50 | LPD ($\times 10^3$ W m$^{-3}$) | 2.14 | 2.22 | 2.30 | 2.28 |
| | | | ET (s) | 488 | 728 | 799 | 813 |
| | | | NC ($\times 10^9$ nps/ml) | 7.00 | 6.50 | 6.10 | 6.00 |
| 50 | 100 | 50 | LPD ($\times 10^3$ W m$^{-3}$) | 2.99 | 2.80 | 2.89 | 2.90 |
| | | | ET (s) | 335 | 536 | 583 | 587 |
| | | | NC ($\times 10^9$ nps/ml) | 4.60 | 5.80 | 5.70 | 5.60 |
| 50 | 50 | 100 | LPD ($\times 10^3$ W m$^{-3}$) | 3.00 | 2.82 | 2.82 | 2.79 |
| | | | ET (s) | 469 | 688 | 737 | 746 |
| | | | NC ($\times 10^9$ nps/ml) | 3.80 | 4.40 | 4.60 | 4.50 |

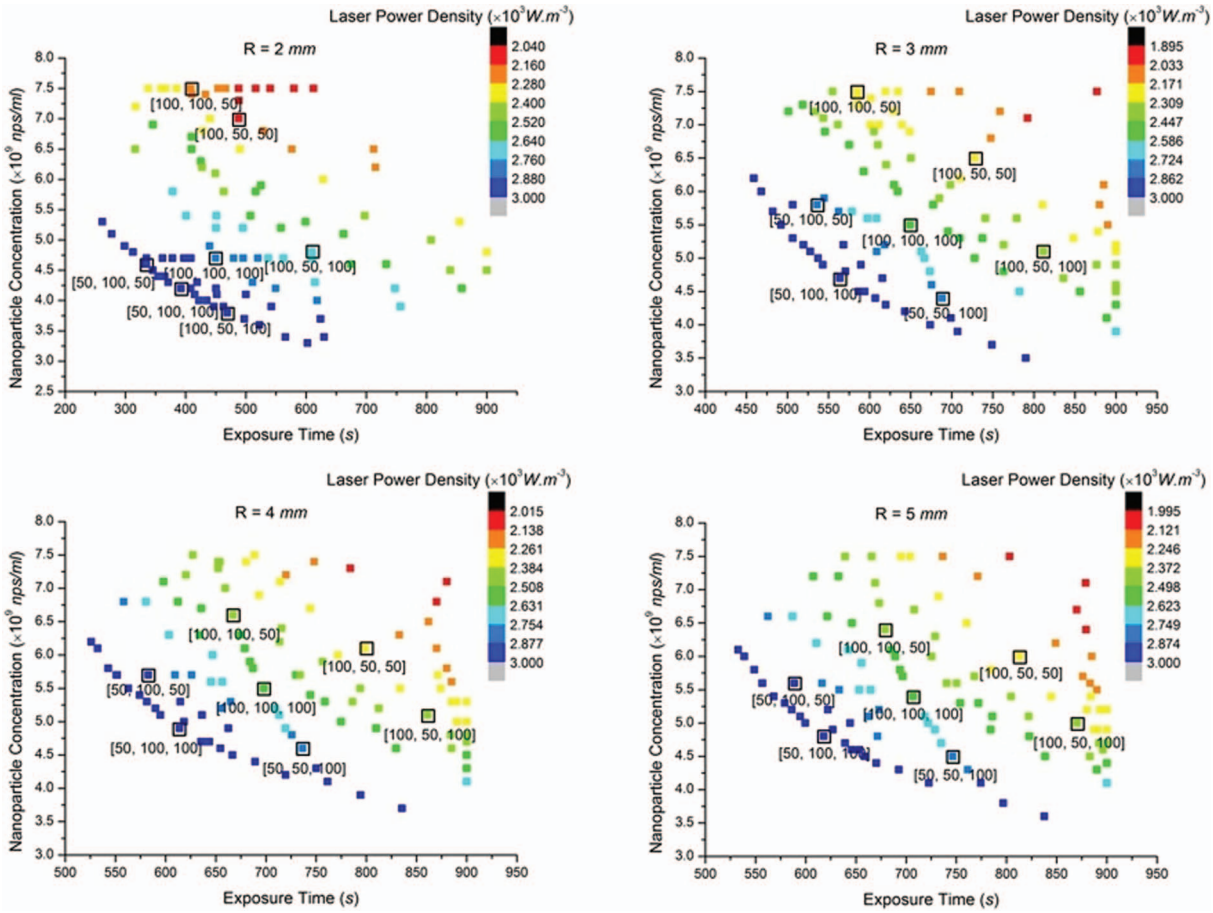


FIG. 6. Optimized values of the laser power density (W m$^{-3}$), exposure time (s), and nanorod concentration ($\times 10^9$ nps/ml) for weights from 20 to 100 in a step size of 20 and for weights from 50 to 100 in a step size of 50, for tumors of different sizes.

in the normal tissue is easily achievable by varying the free parameters. By manipulating the parameters involved such as laser power density, exposure time, and nanorod concentration, one can optimize the extent of the desired thermal damage in the region. However, there is a limited range of these parameters where the desired treatment outcome can be achieved and the optimization method developed in this study can find such ranges according to the clinician's preference about which parameter(s) need to be optimized in terms of priority.

From the optimization results for various weight sets in Table II, it is noticed that a slight decrease in one free parameter can be compensated by an increase in other free parameters and vice versa, in which the desired thermal damage can always be achieved. Furthermore, Fig. 6 shows that at higher power densities, the optimized nanorod concentration and the exposure time have a fairly limited range. However, when the laser power density decreases the optimized values of two other parameters cover a broader range. This infers the importance of optimization in PPTT, which provides flexibility for a clinician to make appropriate choice for specific patients according to their special needs. For example, a lower laser power density and/or a shorter laser exposure time might be preferable for a patient sensitive to laser illumination. A lower nanoparticle concentration is preferred for a patient who is potentially allergic to nanoparticles.

Depending on the tumor location and size, the treatment can be planned well in advance before the actual experiment by the proposed computational methodology. The initial values of the parameters can be selected using this method before the start of the actual treatment. Furthermore, by using *in vivo* measurement tools to provide an instant map of the spatiotemporal temperature elevation and thermal damage in the tumor during laser therapy, the methodology demonstrated in this work could be used to adjust treatment dosage instantly.

## 5. CONCLUSION

In our present study, we numerically investigated the optimization of interstitial plasmonic photothermal therapy for spherical tumors. The spatiotemporal distribution of temperature elevation and thermal damage for the tumor model with a given concentration of nanorods interstitially irradiated with near-infrared laser light was simulated using a commercial software package based on the finite element method, COMSOL Multiphysics. A novel objective function with a tunable weight for each parameter was created to enable the optimization of multiple key parameters, including nanoparticle concentration, laser power density, and exposure time, simultaneously but with different levels of priority. A thermal damage value of one calculated by Arrhenius damage law, which is more accurate than a threshold temperature typically used for characterizing thermal damage, was used to indicate effective treatment. The optimization study has demonstrated the feasibility of optimizing the damage pattern in the tumor treatment. It has been shown that through optimization, different combinations of the parameters can yield similar desired damage to a particular sized tumor. This process can significantly improve the treatment outcome, especially when the tumor is deeply seated and regularly shaped. We believe that the current study has the potential to provide guidance to clinicians in designing individualized protocols in interstitial plasmonic photothermal therapy for cancer patients.

## ACKNOWLEDGMENT

The authors gratefully acknowledge the financial support from ASTAR-ANR joint grant (Grant No. 102 167 0115), funded by the ASTAR-SERC (Agency for Science Technology and Research, Science and Engineering Research Council) in Singapore.

[a]Author to whom correspondence should be addressed. Electronic mail: quanliu@ntu.edu.sg

[1]X. Huang, P. K. Jain, I. H. El-Sayed, and M. A. El-Sayed, "Plasmonic photothermal therapy (PPTT) using gold nanoparticles," Lasers Med. Sci. **23**, 217–228 (2008).

[2]S. Kessentini and D. Barchiesi, "Quantitative comparison of optimized nanorods, nanoshells and hollow nanospheres for photothermal therapy," Biomed. Opt. Exp. **3**(3), 590–604 (2012).

[3]L. R. Hirsch, R. J. Stafford, J. A. Bankson, S. R. Sershen, B. Rivera, R. E. Price, J. D. Hazle, N. J. Halas, and J. L. West, "Nanoshell-mediated near-infrared thermal therapy of tumors under magnetic resonance guidance," Proc. Natl. Acad. Sci. U.S.A. **100**, 13549–13554 (2003).

[4]S. Krishnan, P. Diagaradjane, and S. H. Cho, "Nanoparticle-mediated thermal therapy: Evolving strategies for prostate cancer therapy," Int. J. Hyperthermia **26**(8), 775–789 (2010).

[5]E. B. Dickerson, E. C. Dreaden, X. Huang, I. H. El-Sayed, H. Chu, S. Pushpanketh, J. F. McDonald, and M. A. El-Sayed, "Gold nanorod assisted near-infrared plasmonic photothermal therapy (PPTT) of squamous cell carcinoma in mice," Cancer Lett. **269**(1), 57–66 (2008).

[6]G. P. Goodrich, L. Bao, K. L. Gill-Sharp, J. Wang, and J. D. Payne, "Photothermal therapy in a murine colon cancer model using near-infrared absorbing gold nanorods," J. Biomed. Opt. **15**(1), 018001 (2010).

[7]A. Masters and S. G. Bown, "Interstitial laser hyperthermia," Semin. Surg. Oncol. **8**, 242–249 (1992).

[8]T. Schroder, M. Castren-Persons, A. Lehtinen, and M. Taavitsainen, "Percutaneous interstitial laser hyperthermia in clinical use," Ann. Chir. Gynaecol. **83**, 286–290 (1994).

[9]A. C. Steger, W. R. Lees, K. Walmsley, and S. G. Bown, "Interstitial laser hyperthermia: A new approach to local destruction of tumours," Br. Med. J. **299**, 362–365 (1989).

[10]S. G. Bown, "Phototherapy of tumours," World J. Surg. **7**, 700–709 (1983).

[11]R. J. Stafford, A. Shetty, A. M. Elliott, J. A. Schwartz, G. P. Goodrich, and J. D. Hazle, "MR temperature imaging of nanoshell mediated laser ablation," Int. J. Hyperthermia **27**(8), 782–790 (2011).

[12]A. J. Welch, "The thermal response of laser irradiated tissue," IEEE J. Quantum Electron. **20**, 1471–1481 (1984).

[13]X. Li, S. Fan, Y. Zhao, and S. Xiao, "A numerical simulation of photothermal response in laser medicine," Chin. Opt. Lett. **02**(03), 157–159 (2004).

[14]D. R. Wyman and W. M. Whelan, "Basic optothermal diffusion theory for interstitial laser photocoagulation," Med. Phys. **21**, 1651–1656 (1994).

[15]S. C. Jiang and X. X. Zhang, "Dynamic modelling of photothermal interactions for laser-induced interstitial thermotherapy: Parameter sensitivity analysis," Lasers Med. Sci. **20**, 122–131 (2005).

[16]A. Elliott, J. S. Schwartz, J. Wang, A. Shetty, C. Bougoyne, D. O'Neal, J. Hazle, and R. J. Stafford, "Quantitative comparison of delta P1 versus optical diffusion approximations for modeling near-infrared gold nanoshell heating," Med. Phys. **36**(4), 1351–1358 (2009).

[17]I. L. Maksimova, G. G. Akchurin, B. N. Khlebtsov, G. S. Terentyuk, G. G. Akchurin, I. A. Ermolaev, A. A. Skaptsov, E. P. Soboleva, N. G. Khlebtsov, and V. V. Tuchin, "Near-infrared laser photothermal therapy of cancer by using gold nanoparticles: Computer simulations and experiment," Med. Laser Appl. **22**(3), 199–206 (2007).

[18]X. Xu, A. Meade, and Y. Bayazitoglu, "Numerical investigation of nanoparticle-assisted laser-induced interstitial thermotherapy toward tumor and cancer treatments," Laser Med. Sci. **26**, 213–222 (2011).
[19]M. N. Rylander, Y. Feng, Y. Zhang, J. Bass, R. J. Stafford, A. Volgin, J. D. Hazle, and K. R. Diller, "Optimizing heat shock protein expression induced by prostate cancer laser therapy through predictive computational models," J. Biomed. Opt. **11**(4), 041113–041116 (2006).
[20]M. N. Rylander, Y. Feng, J. Bass, and K. R. Diller, "Heat shock protein expression and injury optimization for laser therapy design," Lasers Surg. Med. **39**(9), 731–746 (2007).
[21]D. Fuentes, J. T. Oden, K. R. Diller, J. D. Hazle, A. Elliott, A. Shetty, and R. J. Stafford, "Computational modeling and real-time control of patient-specific laser treatment of cancer," Ann. Biomed. Eng. **37**(4), 763–782 (2009).
[22]Y. Feng, D. Fuentes, A. Hawkins, J. Bass, M. N. Rylander, A. Elliot, A. Shetty, R. J. Stafford, and J. T. Oden, "Nanoshell-mediated laser surgery simulation for prostate cancer treatment," Eng. Comput. **25**, 3–13 (2009).
[23]H. H. Pennes, "Analysis of tissue and arterial blood temperatures in the resting forearm," J. Appl. Physiol. **1**, 93–122 (1948).
[24]N. T. Wright, "On a relationship between the Arrhenius parameters from thermal damage studies," J. Biomech. Eng. **125**, 300–304 (2003).
[25]A. J. Welch and M. J. C. van Gemert, *Optical-Thermal Response of Laser-Irradiated Tissue*, 2nd ed. (Springer, 2011).
[26]M. S. Skinner, M. N. Iizuka, M. C. Kolios, and M. D. Sherar, "A theoretical comparison of energy sources-microwave, ultrasound and laser- for interstitial thermal therapy," Phys. Med. Biol. **43**, 3535–3547 (1998).
[27]J. Vera and Y. Bayazitoglu, "Gold nanoshell density variation with laser power for induced hyperthermia," Int. J. Heat Mass Transfer **52**, 564–573 (2009).
[28]J. Joseph, V. M. Murukeshan, and L. S. Woh, "Effect of composition, dimension and shape on the optical properties of gold nanoparticles—A theoretical analysis," Am. Soc. Eng. Manage. **3**(3), 188–196 (2011).
[29]M. F. Marqa, P. Colin, P. Nevoux, S. R. Mordon, and N. Betrouni, "Focal laser ablation of prostate cancer: Numerical simulation of temperature and damage distribution," Biomed. Eng. Online **10**, 45 (2011).
[30]A. Datta and V. Rakesh, *An Introduction to Modeling of Transport Processes* (Cambridge University Press, New York, 2010).
[31]J. M. Bertram, D. Yang, M. C. Converse, J. G. Webster, and D. M. Mahvi, "Antenna design for microwave hepatic ablation using an axisymmetric electromagnetic model," Biomed. Eng. Online **5** (2006).
[32]B. N. Khlebtsov, E. V. Panfilova, G. S. Terentyuk, I. L. Maksimova, A. V. Ivanov, and N. G. Khlebtsov, "Plasmonic nanopowders for photothermal therapy of tumors," Langmuir **28**, 8994–9002 (2012).
[33]X. Huang, X. Peng, Y. Wang, D. M. Shin, M. A. El-Sayed, and S. A. Nie, "A reexamination of active and passive tumor targeting by using rod-shaped gold nanocrystals and covalently conjugated peptide ligands," ACS Nano **4**(10), 5887–5896 (2010).
[34]Y. Chen, J. Zhnag, J. Dai, X. Feng, H. Lu, and C. Zhou, "Angiogenesis of renal cell carinoma: Perfusion CT findings," Abdom. Imaging **35**(5), 622–628 (2010).
[35]T. M. Baran, J. D. Wilson, S. Mitra, J. L. Yao, E. M. Messing, D. L. Waldman, and T. H. Foster, "Optical property measurements establish the feasibility of photodynamic therapy as a minimally invasive intervention for tumors of the kidney," J. Biomed. Opt. **17**(9), 098002–098001 (2012).
[36]A. F. Emery and K. M. Sekins, "The use of heat transfer principles in designing optimal diathermy and cancer treatment modalities," Int. J. Heat Mass Transfer **25**, 823–834 (1982).
[37]K. Giering, J. Lamprecht, and O. Minet, "Specific heat capacities of human and animal tissues," Proc. SPIE **2624**, 188–197 (1995).
[38]H. Ying, S. Minoru, L. Hao, H. Ryutaro, and S. Zhigang, "A numerical coupling model to analyze the blood flow, temperature, and oxygen transport in human tumor under laser irradiation," Comput. Biol. Med. **36**, 1336–1350 (2006).
[39]E. Y. K. Ng and N. M. Sudharsan, "An improved three-dimensional direct numerical modelling and thermal analysis of a female breast with tumour," J. Eng. Med. **215**, 25–37 (2001).
[40]S. A. Sapareto, *Physical Aspects of Hyperthermia*, edited by G. Nussbaum (American Institute of Physics, 1982), Chap. 1.
[41]J. Vera and Y. Bayazitoglu, "A note on laser penetration in nanoshell deposited tissue," Int. J. Heat Mass Transfer **52**, 3402–3406 (2009).
[42]B. Jang, Y. S. Kim, and Y. Choi, "Effects of gold nanorod concentration on the depth-related temperature increase during hyperthermic ablation," Small **7**(2), 265–270 (2010).
[43]B.-M. Kim, S. L. Jacques, S. Rastegar, S. Thomsen, and M. Motamedi, "Nonlinear finite-element analysis of the role of dynamic changes in blood perfusion and optical properties in laser coagulation of tissue," IEEE J. Sel. Top Quantum Electron. **2**, 922–933 (1996).
[44]M. N. Iizuka, I. A. Vitkin, M. C. Kolios, and M. D. Sherar, "The effects of dynamic optical properties during interstitial laser photocoagulation," Phys. Med. Biol. **45**, 1335–1357 (2000).